Ultrasensitive On-Site Detection of Biological Active Ricin in Complex Food Matrices Based on Immunomagnetic Enrichment and Fluorescence Switch-On Nanoprobe

Jiefang Sun,[†] Xueyong Zhang,[§] Ting Li,[∥] Jijia Xie,[⊥] Bing Shao,[*,†,‡] Dingshuai Xue,[#] Xu Tang,[#] Hui Li,[†] and Yanhong Liu[#]

[†]Beijing Key Laboratory of Diagnostic and Traceability Technologies for Food Poisoning, Beijing Center for Disease Prevention and Control, Beijing 100013, P. R. China

[‡]Beijing Advanced Innovation Center for Food Nutrition and Human Health, China Agricultural University, Beijing 100193, P. R. China

[§]School of Police Law Enforcement Abilities Training, People's Public Security University of China, Beijing 100038, P. R. China

[∥]School of Public Health, Capital Medical University, Beijing 100069, P. R. China

[⊥]Department of Chemical Engineering, University College London, Torrington Place, London WC1E7JE, United Kingdom

[#]State Key Laboratory of Lithospheric Evolution, Institute of Geology and Geophysics, Chinese Academy of Sciences, Beijing 100029, P. R. China

ABSTRACT: Ricin is a highly toxic protein largely existing in castor beans, which could be used as a warfare agent due to its unique properties. As a deadenylase, inactivation of ricin means a loss of its toxic threat. Therefore, developing simple, accurate, and sensitive on-site detection of biologically active ricin in wide types of complex matrices is most valuable. Here, antifouling polymer brush modified magnetic beads were prepared first and post modified with ricin monoclonal antibody (the MB@P(C−H)-mAb$_{ricin}$) to efficiently capture ricin from various foods and biological matrices. Active ricin obtained in this manner were sequentially determined by a new designed AuNP/QDs nanoassembly. In this double strand oligodeoxynucleotides (dsODN) linked core−satellite nanoprobe, the fluorescence of satellite QDs was extensively quenched by AuNPs due to the dipole−metal interaction. Active ricin can react with its specific depurination substrates which had been inserted in the dsODN linkers. This reaction would trigger the separation of QDs from Au cores by cutting multiple adenines, and then result in the restoration of QDs fluorescence. By coupling with the magnetic enrichment, this AuNP/QDs nanoprobe provided a qualitative result for active ricin in the range from 10.0 to 100.0 ng mL^{-1} with the limit of detection as low as 7.46 ng mL^{-1}. Compared with previously proposed methods, this on-site detection strategy offered an easy to handle on-site test for trace amounts of active ricin in a wide range of complex matrices.

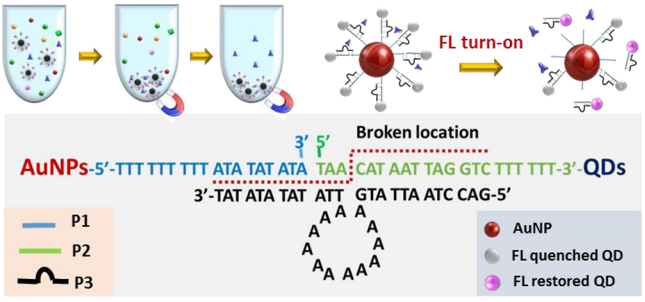

Ricin is a highly lethal natural toxin found in the seed of the castor bean plant, *Ricinus communis*. Ricin belongs to type II ribosome-inactivating proteins. It contains both a deadenylase A chain and a galactose receptor-binding B chain linked by a disulfide bond in the protein structure. Active ricin enters eukaryotic cells via the B chain mediated endocytosis and subsequently the A chain depurinates a specific adenine from 28S rRNA, which induces the failure of protein synthesis and finally activates cell death pathway.[1−3] This biological process is so efficient that a single active ricin can inactivate 1500 ribosomes/min.[1] Therefore, the lethal dosage of ricin in human is approximately 5−10 μg kg^{-1} (per kilogram of body weight) through inhalation and 1−20 mg kg^{-1} body weight when ingested.[2,3] Due to its easy accessibility, high lethality, wide pH tolerance as well as good thermostability, ricin had been listed in Schedule 1 chemicals by the Chemical Weapons Convention (CWC) as the only protein biotoxin since 1997.[4,5] Besides, the United States Centers for Disease Control and Prevention had also identified ricin as a Category B agent, indicating deliberately it to poison, sabotage, or contaminate various environmental sources even foods.[6,7] Although its production, possession, and use have been strictly regulated, ricin still appeared in several terrorist attacks occurring in London and Washington, DC in 2003, as well as in the White

Scheme 1. Overall Detecting Process of This Method for Active Ricin: (A) Synthesis of the MB@P(C−H)-mAb$_{ricin}$; (B) Recovery of Ricin from Complex Samples under External Magnetic Field; and (C) Sensing Principle of the AuNP/QDs Nanoprobe for Active Ricin

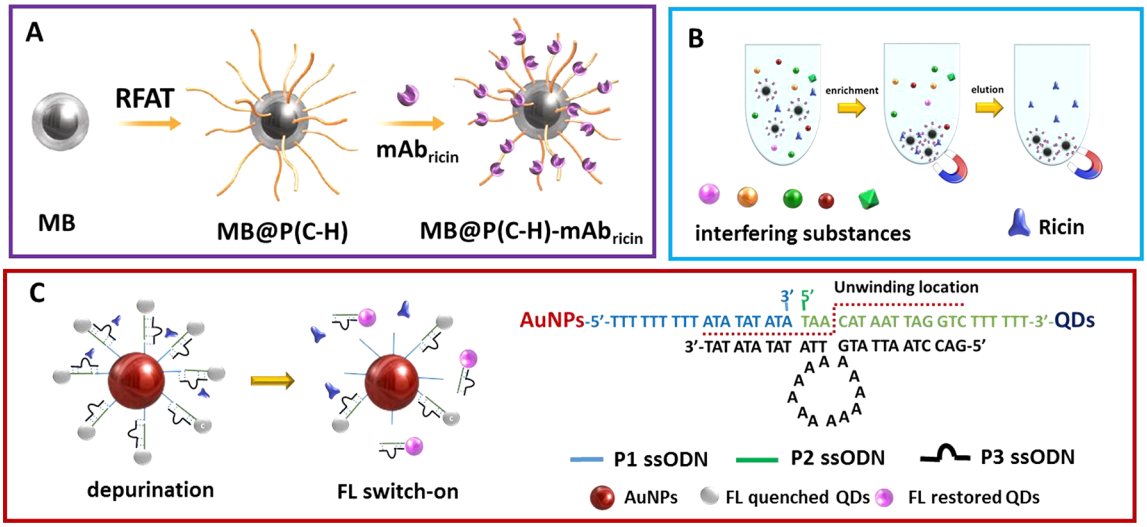

House in 2013, respectively.[8,9] Recently, the claims that ricin could have been potentially used in attacking urban populations were also disputed.[10] Therefore, unambiguous identification of this biological agent in complex matrices is of utmost importance in both food safety protection and antibioterrorism.

Direct identification of ricin has been extensively investigated using reliable laboratory instruments, such as liquid chromatography tandem mass spectrometry (LC-MS/MS) or matrix assisted laser desorption ionization time-of-flight mass spectrometry (MALDI-TOF/MS).[11,12] In the past decade, rapid development of nanomaterials offered versatile building blocks for constructing ricin specific nanobiosensors based on antibody or aptamer recognition, which were detected by electrochemical,[13] surface plasmon resonance,[14] surface-enhanced Raman spectroscopy,[15,16] or fluorescence detection.[17,18] These novel nanoprobes provided diversified potential options for ricin recognition. However, their inherent drawbacks of failing to determine active ricin limited their real applications.

Actually, detecting biologically active ricin has more value in timely assessing a ricin threat, because inactivation means a loss of toxicity. Current analytical methods for active ricin are based on detecting released adenines from the synthetic DNA/RNA mimic of the toxin's natural rRNA target by LC-MS,[19] MALDI-TOF/MS,[20] or chemiluminescenece.[21] In addition, some cell-based bioassays have also been developed for active ricin analysis.[22,23] In these assays, strong dependency on laboratory facilities and operators' skills significantly restricted them in on-field testing. Although some simple and sensitive active ricin detecting strategies have been proposed based on SERS[24] or colorimetric detection,[25] they showed powerlessness when they were used in complex food matrices. In order to cooperate with rapid and proper medical treatments or decontamination, it still needs considerable efforts in constructing reliable on-field active ricin assays with excellent matrix-adaptability to assess potentially hazardous situations in various suspicious contaminated foods and biological samples.

Fluorescence assays relied on portable spectrometers or the naked eye are acknowledged in their rapid, simple, and sensitive signal feedbacks, which make them quite applicable in on-field detection.[26−29] Over the past decade, quantum dots (QDs) have received great attention due to their unique fluorescent properties. Compared with organic fluorophores, QDs offer the excellent advantages of flexible bioconjugation, strong and stable luminescence, as well as adaptable assembly capacity,[30−33] all of which facilitated their wide application in biological labeling, chemical sensing, and bioimaging. Especially, incorporating QDs with gold nanoparticles (AuNPs) via self-assembly has been demonstrated to be an effective resolution for fabricating various target-specific nanosensors.[34−36] Although the fluorescence signal is sensitive, its susceptibility to interference would unavoidably detract from the detection accuracy.[37] Here, a sensitive and reliable on-site detection strategy was proposed by integrating a ricin-specific magnetic adsorbent with a fluorescence switch-on nanoprobe. The overall working principles are illustrated in Scheme 1. On the basis of a typical reversible addition−fragmentation chain transfer (RFAT) polymerization, nonfouling polymer brushes (P(C−H)) composed of both carboxy-functional zwitterionic carboxybetaine methacrylamide (CBMAA) and nonionic hydroxypropyl methacrylamide (HEMA) were grafted from the MBs, and then postmodified with the ricin monoclonal antibody (mAb$_{ricin}$). The presence of the P(C−H) interface on the MBs could well integrate fouling resistance with high recognition element immobilization capacity, therefore it showed an excellent capturing ability for trace amount of ricin in complex matrices. Particularly, in the AuNP/QDs nanoprobe, the ssODN-1 (P1) functionalized Au NPs (the P1-AuNPs) and the ssODN-2 (P2) modified QDs (the P2-QDs) were linked by hybridizing them with the third ssODN-3 (the P3) which contained a specific ricin depurination substrate, i.e., poly(dA$_{12}$) to fabricate a core−satellite nanoassembly, thus the fluorescence of QDs were quenched due to the dipole−metal interaction. The active ricin was first enriched by a magnet, and subsequently eluted and determined by the AuNP/QDs nanoprobe based on its specific depurination reaction. In the presence of active ricin, it would cut multiple adenines from both the poly(dA$_{12}$) loops and the dsODN linkers between the P1-AuNPs and the P3, and then triggered a dissociation of the

P2-QDs from the P1-AuNPs. As a consequence, the concentration of active ricin could be simply determined by monitoring FL enhancement. By integrating the MB@P(C−H)-mAb_{ricin} adsorbent with the AuNP/QDs nanoprobe, interfering components were unable to disturb the fluorescence signal. Owing to its convenience, high sensitivity, and reliability, this assay could thereby be a promising option for on-site detecting active ricin in various foods and biological samples.

MATERIALS AND METHODS

Chemicals and Instruments. All of ODN were purchased from Shanghai Sangon Biotechnology Co., Ltd. (Shanghai, China) and purified through high-performance liquid chromatography (HPLC). They were listed as follows: (1) P1, the ssODN modified on the surface of AuNPs, i.e., 5′-SH-C_6H_{12}-TTT TTT TTT ATA TAT ATA-3′, with a segmental sequence hybridized with the P3 which was highlighted by underlining and a poly(dT_9) as a spacer sequence, respectively; (2) P2, i.e., the ssODN linked on the surface of QDs with a segmental sequence as the capture strand to hybridize with the P3 (the sequence was highlighted with italic) and a poly(dT_6) as a spacer sequence, i.e., 5′-*TAA CAT AAT TAG GTC* TTT TTT-C_6H_{12}−NH_2-3′; (3) P3: the ssODN contained a special active ricin depurination substrate (poly(dA_{12})) which was highlighted in bold, as well as two sequences which were hybridized with the P1 (highlighted with underline) and the P2 (highlighted with italic), respectively, i.e., 5′-*GAC CTA ATT ATG* **AAAAAAAAAAAA** *TTA* TAT ATA TAT-3′. Intact ricin with purity exceeding 95% by SDS-PAGE analysis was extracted from castor beans following standard procedures.[38] The water-soluble QDs (the ZnS-capped CdSe QDs, modified with the thioglycolic acid) was the product of Wuhan Jayuan Quantum Dots Co. Ltd. (Wuhan, P.R. China). Ricin alpha monoclonal antibody (mAb_{ricin}, RA999) which specifically recognizes the ricin toxin RCA60 was the product of Thermo Scientific (Catalog # MA1−74237). Bis(*p*-sulfonatophenyl)-phenyl phosphine dehydrate dipotassium salt (BSPP) was purchased from the Sigma-Aldrich. Deionized water purified by a Milli-Q water purification system (Millipore, MA, U.S.A.) was used throughout these experiments. The morphology of nanoparticles were observed with a transmission electron microscopy (TEM, JEM-2000EX, Japan). FT-IR spectra were collected on a FT-IR spectrometer (Bruker Vertex 70). Powder X-ray diffraction (XRD) patterns of the as-prepared MBs were recorded using a Rigaku smart lab (Rigaku, Japan) with Cu Kα radiation (λ = 1.5406 Å). Zeta potentials and hydrodynamic sizes were measured on a Malvern Nanosizer instrument (Malvern Instruments, Ltd., U.K.). A Physical Property Measurement System (PPMS) device (Cryogenic, 12 T Magnet) was used to measure magnetic properties of the magnetic beads. Thermogravimetric analysis (TGA) was performed on a TA Instruments device (Model TGA Q500) from room temperature to 800 °C. The UV−vis absorption spectroscopy were collected on a Shimadzu 3600 UV−vis−NIR spectrometer, while the fluorescence spectra was collected on a Shimadzu RF-5301PC.

Preparation of the Specific Magnetic Adsorbent for Ricin. The water dispersible SiO_2 capped Fe_3O_4 microbeads (MBs) and the amino modified MBs (NH_2-MBs) were prepared according to the previously reported method.[39] The monomers, i.e., carboxy-functional zwitterion carboxybetaine methacrylamide (CBMAA)[40] and the silane functionalized RAFT initiator, i.e., propyl-4-(trimethoxysilyl)benzyl carbonotrithioate (CTA) were synthesized according to the reported methods.[41] The detailed synthesis procedures of both CBMAA and CTA are given in the Supporting Information, SI. The copolymer brush grafted MBs (the MB@P(C−H)) were synthesized via a RAFT polymerization (see the SI). Moreover, the sole P(C−H) was also prepared for comparison (see the SI). Finally, the ricin-specific MBs (the MB@P(C−H)-mAb_{ricin}) were prepared by covalently linking the mAb_{ricin} on the MB@P(C−H) via a typical EDC active amino-carboxyl coupling procedures (see the SI).

Measuring the Adsorption Affinity of the MB@P(C−H)-mAb_{ricin} to Ricin. For extracting ricin, 10 mg of the MB@P(C−H)-mAb_{ricin} was added to a series of standard solutions (1.0 mL) with the ricin concentrations ranged from 10 to 50 μg mL^{-1}. After incubating 2 h, the equilibrium concentrations of ricin in the supernatants were determined by the BCA protein assay. In addition, the binding kinetic between ricin and the MB@P(C−H)-mAb_{ricin} was examined by mixing 10 mg of the MB@P(C−H)-mAb_{ricin} with 50 μg ricin in 1.0 mL PBS buffer. At different incubating times from 20 to 120 min, the concentrations of ricin in the supernatant were determined by the BCA protein assay. The equilibrium adsorption amount (Q) of the MB@P(C−H)-mAb_{ricin} was calculated based on the equation below:

$$Q = (C_0 - C_e) \times V \times m^{-1} \times 10^3 \text{ (mg/g)}$$

Here, C_0 (μg mL^{-1}) represents the initial ricin concentration in PBS buffer; C_e (μg mL^{-1}) is the equilibrium concentration of ricin in the supernatant; V (mL) is the volume of sample solution; and m (g) is the mass of the MB@P(C−H)-mAb_{ricin}.

Construction of the AuNP/QDs Nanoprobe. AuNPs with diameter of ca. 60 nm were synthesized based on the seed-growth method.[42] According to this research, the concentration of AuNP sol after 6 growth steps is nearly 1.9 × 10^{11} (NP mL^{-1}). For stabilizing AuNPs, BSPP (15 mg) was added to the AuNP sol (100 mL) under stirring and then reacted for another 10 h.[43] The P1 modified AuNPs (the P1-AuNPs) were obtained via the strong binding between Au and thiol (the detail modifying process was described in the SI).[44] Finally, the P1-AuNPs dispersed in buffer solution (10 mM PBS, pH 7.4) were standardized to 10 nmol L^{-1}. The P2 modified QDs (the P2-QDs) were prepared using the EDC/sulfo-NHS cross-linking procedure as described in the SI. The fabrication of the AuNP/QDs nanoprobe was carried out in the hybridization buffer solution (10 mM PBS pH 7.4, 5 mM $MgCl_2$, 0.01% Tween 20). Typically, the P1-AuNPs, the P2-QDs and the P3 were mixed at a molar ratio of 1:50:200. The hybridization-assistant assembly was conducted first under 80 °C for 10 min and then at 37 °C for another 2 h, thus obtaining the fluorescence-quenched AuNP/QDs nanoprobe. The AuNP/QDs were purified by centrifuge and suspended in 10 mM PBS buffer for further use. In addition, AuNPs were deposited on clear Si wafers by evaporating the aqueous phase, providing films used to collect SERS signals.

Sensing Active Ricin Using the AuNP/QDs Nanoprobe. The AuNP/QDs solution was standardized to 0.5 OD at 535 nm using the UV−vis spectroscopy. For quantitation, a certain amount of ricin was dispersed in the TFA/DI water/ethanol (1:50:49 (v/v/v) for 30 min and then added into the AuNP/QDs nanoprobe solution (200 μL, 0.5 OD). After incubation at 38 °C for 2 h, the fluorescence of these solutions were measured. To monitor the depurination kinetic between

active ricin and the AuNP/QDs nanoprobe, this sensing solution contained active ricin (100 ng mL^{-1}) and the AuNP/QDs nanoprobe (0.5 OD) underwent fluorescence tests every 20 min until the signal reached a stable value. After determining the fluorescence intensity, all of these solutions were ultrafiltered to obtain the nanoparticle-free filtrates. The released adenines in the filtrates were also measured by LC-ESI-TOF/MS (the detailed testing procedures are given in the SI). The specificity of the AuNP/QDs nanoprobe to some interfering proteins was tested individually using the same method as that for detecting active ricin.

Selective Detection of Active Ricin from Various Complex Matrices. Various complex food and biological samples including orange juice, ham, sandwich, milk, coffee, and human plasma serum were used to evaluate the applicability of the proposed detection strategy, which were all spiked with ricin (the sample preparation procedures are given in the SI). Specifically, 10 mg of the MB@P(C−H)-mAb_{ricin} were directly mixed with 1.0 mL of the ricin-spiked samples. For ensuring a full recovery of ricin, a binding time of 1 h was used for capturing ricin in real samples, and the supernatant was decanted by easy separation with a magnet. After washing with PBST and PBS buffer, the elution solution of TFA/DI water/ethanol (1:50:49 (v/v/v), 100 μL) was used to fully elute ricin from the MB@P(C−H)-mAb_{ricin} for 30 min at 25 °C. After removing the adsorbent, active ricin in the supernatant was quantified using the AuNP/QDs nanoprobe according to the above method. Simultaneously, the recovered ricin was also determined by the proposed LC-MS/MS method[45] as comparison (please see SI). The recoveries in each sample were calculated by comparing the determined concentrations with that of the added one.

RESULTS AND DISCUSSION

Fabrication and Characterization of the P(C−H) grafted MBs.

Challenges for nanomaterial-based sensing are associated with severe interference in complex samples and nonspecific fouling in the nanosensing interface. This effect would lead to false negative results, thus creating difficulties in target identification. Therefore, great attention has been devoted to the integration of sample preparation with an analysis step to provide fast and reliable assay. CBMAA, which has been reported as a key monomer in fabricating an ultralow fouling interface, was copolymerized randomly with a nonionic HEMA monomer, which composed flexible three-dimensional polymer brushes around MBs (the MB@P(C−H)). As determined by XRD, the crystalline structure of the MB@P(C−H) keeps the face-centered cubic spinel structure as that of the Fe_3O_4 NP and the Fe_3O_4@SiO_2 (MBs) precursor, demonstrating that the chemical modifying process did not change its crystalline structure (Figure S1). TEM images (Figure 1A) confirm the well dispersity and uniform morphology of the MB@P(C−H). By zooming in on one particle, it can be easily distinguished that the MB@P(C−H) presents the Fe_3O_4 core of ∼120 nm in diameter, and the middle SiO_2 layer of ∼10 nm as well as the outer P(C−H) brushes of 15−20 nm in thickness (Figure 1B), respectively. As measured by DLS, the average hydrodynamic diameter of the MB@P(C−H) was 182 nm with the DPI of 0.24. With respect to verifying the successful graft of P(C−H) chains on the MBs, FT-IR studies provided important information (Figure 1C). Here, the FT-IR spectra of the sole P(C−H) was given in Figure 1C for comparison. It can be seen that both the MB@P(C−H) and the sole P(C−H) share very similar FT-IR spectra. Notably, there are strong peaks around 1100 cm^{-1} assigned to the Si−O bond which confirms the presence of SiO_2 both in the MBs and the MB@P(C−H). As for the MB@P(C−H), the wide absorption band around 3405 cm^{-1} was attributed to the stretching vibration of −OH. Several bands around 2940−2990 cm^{-1} indicate the presence of the alkane groups. The amide I and II bands locate at about 1653 and 1585 cm^{-1}, respectively. The carboxyl stretching vibration of the −COOH appears at 1721 cm^{-1}. In addition, the peak at 1386 cm^{-1} represents the C−O symmetric stretching band. All of these bands indicated the success graft of the P(C−H) on the MBs. It is shown that the MB@P(C−H) has a weight loss of ∼17% by TGA analysis, which is significantly higher than that of the MBs with less than the 3% weight loss (Figure 1D). Moreover, the saturation magnetization of the MB@P(C−H) was measured as 34.5 emu g^{-1}, and the magnetization curve exhibits symmetry and passes accurately through the origin, which ensures a facile separation and reusability of the MB@P(C−H) from sample matrices.

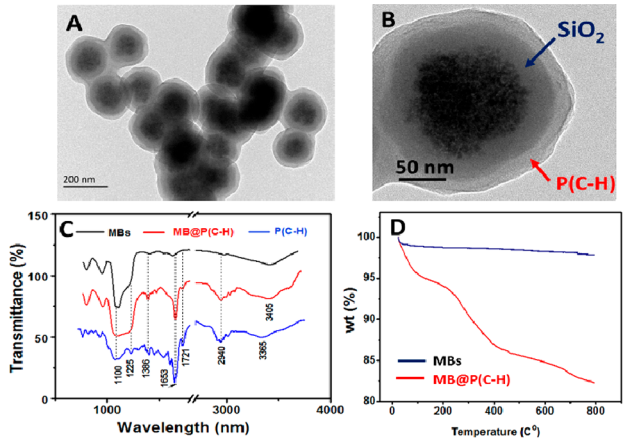

Figure 1. TEM image of the MB@P(C−H) (A) and a zoom-in image of it (B). The arrows in B show different layers around the Fe_3O_4 core; (C) FT-IR spectra of the P(C−H) and the MB@P(C−H); and (D) TGA analysis of the MBs before and after being grafted P(C−H) polymer brushes.

For achieving selective capture, the mAb_{ricin} was covalently linked on the MB@P(C−H) as a recognition element. It is demonstrated that the amount of mAb_{ricin} immobilized on the MB@P(C−H) (each gram of the MB@P(C−H))-mAb_{ricin} contained 28 mg mAb_{ricin}) is nearly three times higher than that of the amino-MBs (each gram of the MBs contained 6.2 mg mAb_{ricin}). The MB@P(C−H)-mAb_{ricin} reached to the saturated adsorption within 20 min, suggesting that the flexible interface of the MB@P(C−H)-mAb_{ricin} facilitated the recognition and binding between mAb_{ricin} and ricin by decreasing steric hindrance, thus achieving fast adsorption balance. It is shown that compared with the reported method[45] which used the TFA/DI water solution (1:99 volume ratio) to elute ricin, the addition of ethanol in the eluent (TFA/DI water/ethanol (1:50:49, volume ratio) shows better eluting efficiency (Table S2 in SI). This difference might come from the special chemical property of the P(C−H) layer on the adsorbent. As shown in Table S2, the MB@P(C−H)-mAb_{ricin} could be effectively applied in various tainted samples, and the recoveries were calculated to be 66%−86% for 20 ng mL^{-1} and 77.0%−92% for 50 ng mL^{-1} ricin, respectively, according to the LC-MS/MS measurements, which suggested the

extraction procedures used in this assay were satisfied. It is also shown that the MB@P(C−H)-mAb$_{ricin}$ was superior to the dual-recognition affinity magnetic adsorbent (the MB@P(ConA/Gal)) proposed by our group[25] in the aspects of both the matrix-adaptability and the recovery rates. It was examined that the MB@P(C−H)-mAb$_{ricin}$ showed weak nonspecific interaction with HSA (less than 84 $\mu g\ g^{-1}$). Benefiting from the presence of the fouling resistant P(C−H) layer, protein interferences could be excluded. All of these results demonstrated that the MB@P(C−H)-mAb$_{ricin}$ exhibited good fouling resistance, high ligand-loading capacity, and high target recovery capacity due to the presence of the P(C−H) interfaces as a scaffold for the mAb$_{ricin}$.

Design and Characterization of the AuNP/QDs Nanoprobe. TEM image reveals that the P1-AuNPs exhibit spherical shapes with the average diameter of ca. 60 nm (Figure 2A). Zeta potentials and hydrodynamic diameters

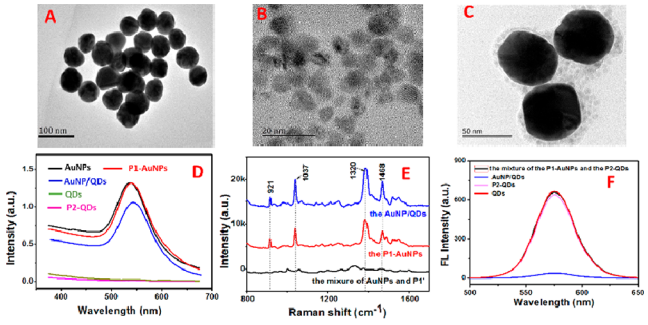

Figure 2. TEM image of the P1-AuNPs (A), the P2-QDs (B), and that of the AuNP/QDs assemblies (C); UV−vis absorption spectra of different modified AuNPs, QDs and that of the AuNP/QDs nanoprobe (D); SERS spectra of the P1-AuNPs and that of AuNP/QDs nanoprobe (E); and (F) fluorescent spectra of the QDs and the AuNP/QDs nanoprobe.

changed from −18.7 mV and 63 nm for the bare AuNPs to −26.5 mV and 68 nm for the P1-AuNPs. As for the P2-QDs, they show spherical shapes with an average diameter of 6 nm in TEM image (Figure 2B). Zeta potential and hydrodynamic diameter before and after conjugation with P2 also showed some changes from −23.7 mV and 10 nm for the bare QDs to −25.4 mV and 14 nm for the P2-QDs. Both the bare QDs and the P2-QDs have very similar absorption spectra, indicating the bioconjugation of the P2 on the QDs did not change their optical properties (Figure 2D). AuNPs and QDs can act as ideal energy acceptors/donors in constructing fluorescence resonance energy transfer (FRET) based nanosensors, due to their excellent optical properties.[46,47] In this work, ODN hybridization was employed to fabricate the core−satellite AuNP/QDs nanoassembly. For achieving an optimized double strand ODN (dsODNs) linker, several dsODN linkers with different lengths and base compositions (Table S3) were designed to examine their depurination reaction with active ricin. It is found that active ricin could cut adenines from these dsODN substrates under pH 4.0, thus inducing the loss of these dsODNs (Figure S2). Considered from both the stability and the sensitivity of the AuNP/QDs nanoprobe, the linker between the P1-AuNPs and the P3 was designed to have the same sequence as that of the S2. In addition, it has been verified that the poly(dA$_{12}$) was the most efficient substrate according to our previous research.[24] Therefore, the poly(dA$_{12}$) was chosen as the depurination substrate in this AuNP/QDs nanoprobe. Active ricin could cut multiple adenines both from the poly(dA$_{12}$) loops and the dsODN linkers between the P1−Au and the P3, finally inducing separation among QDs and AuNPs (the broken site is shown in Scheme 1C). However, the base-pairs between the P3 and the P2-QDs could remain stable during the reaction process. Considered from both the signal-to-noise ratio and the sensitivity of the AuNP/QDs nanoprobe (Figure S3), the feeding molar ratio of the P1-AuNPs, the P2-QDs and the P3 at 1:50:200 was selected in this method. As illustrated in the TEM image (Figure 2C), a number of the P2-QDs are assembled around the P1-AuNPs, and present a core−satellite nanostructure. Simultaneously, the QDs/AuNP nanoassemblies (Figure 1D) display the absorption peak around 543 nm, which show a slight red-shift of 5 nm compared with that of the P1-AuNPs. SERS spectra of the P1-AuNPs exhibit strong Raman features corresponding to ssODN (Figure 2E), i.e., the C−N wagging at 1037 cm^{-1}, the C−N stretching at 1320 cm^{-1}, and COO^- stretching mode at 1468 cm^{-1}, respectively, indicating the presence of ssODN in their structures. All of these typical peaks also show up in the SERS spectra of the AuNP/QDs. However, the SERS spectra of the psychical mixture of the AuNPs and P1′ which had the same sequence as P1 but did not modify the thiol group in the 5′ end show a very weak SERS signal compared to that of the P1-AuNPs, indicating that the ssODN could not efficiently bind to the AuNPs without having a thiol group. In addition, the zeta potential of the AuNP/QDs assembly was measured to be −24.6 mV, and the hydrodynamic diameter of assemblies increased to 96.3 nm. As shown in the Figure 2F, the FL intensity of the physical mixture of the P2-QDs and the P1-AuNPs was measured as 575, which show little change in signal intensity comparing with the same amount P2-QDs solution. After adding the P3, the FL intensity dropped down to 45, suggesting that the fluorescence quenching was attributed to hybridization induced dipole−metal interactions. All of this evidence verified the successful preparation of the AuNP/QDs nanoassembly via hybridization.

Detection of Active Ricin Using the AuNP/QDs Probes. The core−satellite AuNP/QDs nanoprobe was fabricated via ODN hybridization, while its nanostructure could disassemble in the presence of active ricin. TEM images (Figure 3A,B) reveal that more and more QD satellites detach from the core AuNPs with the addition of active ricin. It is deduced that the specific depurination of active ricin toward their substrate sequence, i.e., poly(dA$_{12}$) would make the dsODN linker between the P1-AuNPs and the P3 loose even breakage, thus liberating the QDs from the AuNP core, finally resulting in a fluorescent signal restoration. For verifying this hypothesis, the depurination between active ricin and the AuNP/QDs nanoprobe was also monitored by detecting the unique cleavage product of depurination, i.e., adenine. It was found that the amounts of adenine were well dependent on the concentrations of active ricin (Figure 3C). Moreover, compared with the original ricin, the recovery of ricin scarify parts of their activities due to having been treated with the TFA/DI water/ethanol (1:50:49, volume ratio) eluent, which was reflected by the decreased adenine when reacted with the AuNP/QDs nanoprobe as shown in Figure 3C. Considering the depurination reaction between active ricin and the AuNP/QDs nanoprobe was both time and concentration dependent, a reaction time of 2 h was selected in this assay, thus the FL intensity could be dependent only on the concentration of active ricin. Considering that the decrease of ricin activity after

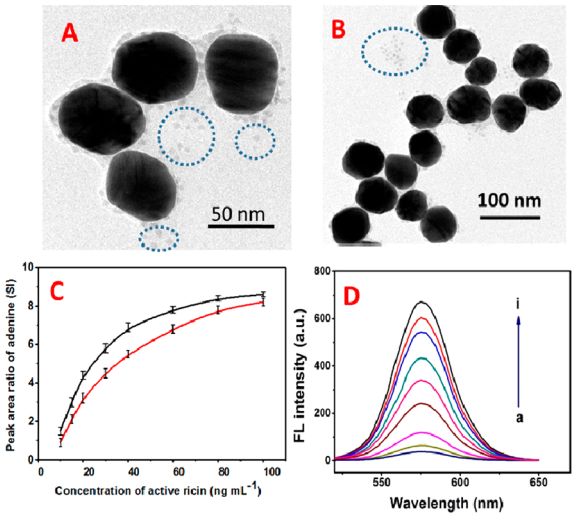

Figure 3. Performances of the AuNP/QDs nanoprobe in buffer solution. TEM images of the AuNP/QDs after adding active ricin (A) 30 ng mL^{-1} and (B) 80 ng mL^{-1}, respectively; (C) concentration of the released adenine after depurination reaction between the AuNP/QDs probes (0.5 OD) and different active ricin before (black line) and after (red line) treated by the elution solutions; and (D) FL spectra of the AuNP/QDs solution upon addition of different concentrations of active ricin (from a to i: 0, 10, 15, 20, 30, 40, 60, 80, and 100 ng mL^{-1}).

elution would cause deviation on quantitative detection, the work curve was built using the ricin pretreated with the same elution process to obtain a consistent activity with the recovery ricin. As shown in Figure 3D, the AuNP/QDs solution displays a gradual fluorescence restoration as a function of increasing concentration of active ricin.

Plotting the increased amplitude of fluorescence at 575 nm (I_{575}) against active ricin concentration yields a Langmuir-type plot that is nonlinear past 100 ng mL^{-1} active ricin, which also indicates that the probe would reach to saturation at higher concentrations. A logarithmic correlation was observed in a wide range of active ricin concentrations from 10 to 100 ng mL^{-1} (Figure 4A). The calibration curve was established as

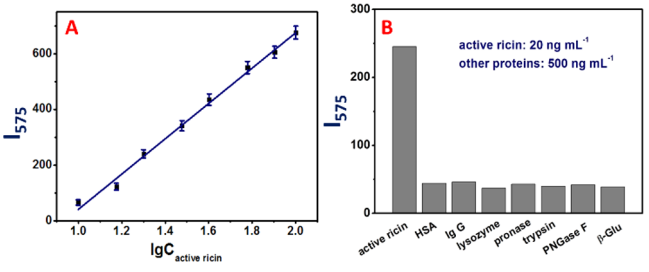

Figure 4. (A) I_{575} plotted against the concentration of active ricin. All error bars were obtained through the detection of six parallel samples. (B) Dependence of I_{575} on different concentrations of interfering proteins.

$I_{575} = 634.8 \times \lg C_{\text{active ricin}} - 594.7$. Here, $C_{\text{active ricin}}$ represents the concentration of active ricin (ng mL^{-1}). The limit of detection (LOD) was calculated to be 7.46 ng mL^{-1} by including the control signal with three times of the standard deviation. The I_{575} gave a relative standard deviation (RSD) of 5.4% by measuring active ricin (50 ng mL^{-1}, $n = 6$), demonstrating the satisfactory reproducibility of the proposed assay. To estimate the specificity of the method, the response of AuNP/QDs nanoprobe to interferences was also examined. It was found that common ions and organic matters did not induce a fluorescent signal turn-on as that of active ricin (data not shown). Some proteins also did not induce fluorescence signal change, demonstrating the good specificity of the method (Figure 4B). However, due to strong electrostatic interaction between positively charged interfering proteins and the negatively charged AuNP/QDs nanoprobe under the optimized reaction condition (pH 4.0). It was found that high concentration coexisted proteins (larger than 5 μg mL^{-1}) could affect the accuracy of this method by forming the large AuNP/QDs aggregates, which further emphasized the necessary of integrating the specific magnetic adsorbent to purify complex samples. Therefore, integrating the MB@P(C−H)-mAb_{ricin} with the AuNP/QDs can greatly extend its application in complex samples.

Analysis of Active Ricin in Spiked Samples. Ricin could contaminate food or drink as it can remain stable even in harsh ambient conditions. To test practical applications of the proposed strategy, enrichment and subsequent detection of active ricin in different foods and biological matrices were conducted. It was found that the MB@P(C−H)-mAb_{ricin} reached saturated adsorption within 20 min, and therefore a binding time of 1 h was used for full capture of ricin in real samples. It was examined that the coexisting TFA (0.1%) and ethanol (4.9%) in the ammonium acetate buffer did not interfere the detection of active ricin (Figure S4). As demonstrated in Table 1, the determination of active ricin

Table 1. Determination of Active Ricin Spiked in Different Matrices by the Proposed Detecting Strategy[a]

		AuNPs/QDs nanoprobe		
sample	spiked (ng mL^{-1})	detected (ng mL^{-1})	recovery (%)	LC-MS (ng mL^{-1})
diluted human serum	20.0	12.4	62.0	14.6
	50.0	38.4	76.8	43.1
	100.0	76.8	76.8	85.4
orange juice	20.0	13.4	67.0	16.8
	50.0	39.5	79.0	44.5
	100.0	79.2	79.2	85.6
ham	20.0	11.6	58.0	13.2
	50.0	34.3	68.6	39.3
	100.0	75.6	75.6	80.8
sandwich	20.0	11.2	56.0	13.7
	50.0	32.7	65.4	38.5
	100.0	73.6	73.6	78.5
milk	20.0	11.8	59.0	15.7
	50.0	37.3	74.6	42.3
	100.0	78.1	78.1	80.2
coffee	20.0	13.8	69.0	15.4
	50.0	39.6	79.2	45.2
	100.0	80.4	80.4	87.5

[a]Data are mean value of 3 measurements.

based on the AuNP/QDs probe were basically coincident with the values measured by the LC-MS/MS method, suggesting the reliability of this newly proposed strategy. According to previous research, the LD50 for human ricin ingestion is estimated at 3 mg kg^{-1} or 105 mg for a 35 kg child. Taking beverages as the example, a deadly oral ingestion of ricin is

approximately 0.4 mg mL^{-1} of 8 oz liquid. That means this newly proposed method can be quantitatively detected for active ricin in the linear range. Moreover, it also can be utilized for simple "yes/no" detection in higher ricin concentration. The AuNP/QDs nanoprobe could also quantatively respond to active ricin even after storage in the PBS buffer for nearly four months under 4 °C (Figure S5), demonstrating its well stability. Compared with different reported active ricin assays (Table S4), this new fluorescence turn-on testing method was simple, sensitive, and accurate, all of these advantages make it apply well to rapid active ricin screening in wide range of complex samples.

CONCLUSIONS

In this work, a fluorescence switch-on assay of active ricin in complex food stuffs was demonstrated by integrating highly efficient immune-affinity magnetic adsorbent with the specific AuNP/QDs nanoprobe. Benefiting from its flexible and adaptive three-dimensional nanostructure, the MB@P(C−H)-mA_{bricin} exhibited increased affinity over both the monolayer mAb_{ricin}-MBs and the dual-recognition MB@P(ConA/G). As an excellent functional magnetic adsorbent, the proposed MB@P(C−H) with high ligand loading capacity and fouling resistance characteristics make them easily fabricate into a wide range of specific adsorbents by conjugating them with various recognition elements, and then easily coupled with the downstream analysis techniques. By integrating them with immune magnetic enrichment, the newly designed AuNP/QDs nanoprobe could provide reliable, low cost, simple, and rapid detection while retaining the top features of the existing rapid on-field assays for active ricin. This strategy holds considerable promise for the emergency requirement of screening the ricin threat in a variety of biodefense and food safety applications.

ASSOCIATED CONTENT

Experimental details for synthesis of the MBs, the NH_2-MBs, the P(C−H) polymer, the MB@P(C−H), the MB@P(C−H)-mAb_{ricin}, the AuNPs, the P1-AuNPs, the P2-QDs as well as the CBMAA, the CTA; the optimization of the feeding ratio for obtaining the best AuNP/QDs nanoprobe, the examination of the long-term stability of the AuNP/QDs, the optimization of the dsODN linker in the AuNP/QDs nanoprobe; the detailed LC-MS/MS method for determining adenine and ricin were also listed; and comparison of different assays available for determining active ricin

AUTHOR INFORMATION

Corresponding Author

*E-mail: shaobingch@sina.com.

Author Contributions

The manuscript was written through the contributions of all authors. All authors have given approval to the final version of the manuscript.

Notes

The authors declare no competing financial interest.

ACKNOWLEDGMENTS

We are particularly grateful to Dr. Jijun Tang and Professor Jianwei Xie for providing ricin. Thank Dr. Chunzheng Li for kindly helping in paper writing. The authors gratefully acknowledge financial support from the National Natural Science Foundation of China (No.U1736201, 21677019 and 41403021), Capital Health Research and Development of Special (2018-4-1014) and the key research and development program of Beijing (D171100008317001).

REFERENCES

(1) Olsnes, S.; Kozlov, J. V. *Toxicon* **2001**, *39*, 1723−1728.
(2) Bradberry, S. M.; Dickers, K. J.; Rice, P.; Griffiths, G. D.; Vale, J. A. *Toxicol. Rev.* **2003**, *22*, 65−70.
(3) Challoner, K. R.; McCarron, M. M. *Ann. Emerg. Med.* **1990**, *19*, 1177−1183.
(4) Select Agents and Toxins. *Code of Federal Regulations, Part 73, Title 42*, 2010, 482.
(5) Schedule 1 Chemicals. *Code of Federal Regulations, Part 712, Title 15*, 2010, Supplement No.1.
(6) Centers for Disease Control and Prevention. *Morb. Mortal. Wkly. Rep.* 2003, *52*, 1129−1131.
(7) Rotz, L. D.; Khan, A. A.; Lillibridge, S. R.; Ostroff, S.; Hughes, M. J. M. *Emerging Infect. Dis.* **2002**, *8*, 225−230.
(8) Hayden, E. C.; Wadman, M. *Guidance Issued for US Internet Research*; US Nature News, Nature Publishing Group: United Kingdom, 2013.
(9) Papaloucas, M.; Papaloucas, C.; Stergioulas, A. *Pak. J. Biol. Sci.* **2008**, *11*, 2370−2371.
(10) Schep, L. J.; Temple, W. A.; Butt, G. A.; Beasley, M. D. *Environ. Int.* **2009**, *35*, 1267−1271.
(11) Brinkworth, C. S. *Anal. Chem.* **2010**, *82*, 5246−5252.
(12) Ostin, A.; Bergstrom, T.; Fredriksson, S. A.; Nilsson, C. *Anal. Chem.* **2007**, *79*, 6271−6278.
(13) Singh, A.; Pasha, S. K.; Manickam, P.; Bhansali, S. *Biosens. Bioelectron.* **2016**, *83*, 162−168.
(14) Stern, D.; Pauly, D.; Zydek, M.; Müller, C.; Avondet, M. A.; Worbs, S.; Dorner, B. G.; Lisdat, F.; Dorner, M. B. *Biosens. Bioelectron.* **2016**, *78*, 111−117.
(15) Szlag, V. M.; Styles, M. J.; Madison, L. R.; Campos, A. R.; Wagh, B.; Sprouse, D.; Schatz, G. C.; Reineke, T. M.; Haynes, C. L. *ACS Sens.* **2016**, *1*, 842−846.
(16) Zengin, A.; Tamer, U.; Caykara, T. *J. Colloid Interface Sci.* **2015**, *448*, 215−219.
(17) Bogomolova, A.; Aldissi, M. *Biosens. Bioelectron.* **2015**, *66*, 290−296.
(18) Xiao, X.; Tao, J.; Zhang, H. Z.; Huang, C. Z.; Zhen, S. J. *Biosens. Bioelectron.* **2016**, *85*, 822−827.
(19) Bevilacqua, V. L.; Nilles, J. M.; Rice, J. S.; Connell, T. R.; Schenning, A. M.; Reilly, L. M.; Durst, H. D. *Anal. Chem.* **2010**, *82*, 798−800.
(20) Wang, D.; Baudys, J.; Barr, J. R.; Kalb, S. R. *Anal. Chem.* **2016**, *88*, 6867−6872.
(21) Sturm, M. B.; Schramm, V. L. *Anal. Chem.* **2009**, *81*, 2847−2853.
(22) Rasooly, R.; He, X. J. *J. Food Prot.* **2012**, *75*, 951−954.
(23) Rastogi, V. K.; Wallace, L. *EPA.* **2010**, *600/R*−10/097. *Novel Cell Based Assay for Testing Active Holo-Ricin and Its Application in Detection Following Decontamination*; U.S. EPA 2010, 600/R-10/097.
(24) Tang, J.; Sun, J.; Lui, R.; Zhang, Z.; Liu, J.; Xie, J. *ACS Appl. Mater. Interfaces* **2016**, *8*, 2449−2455.
(25) Sun, J.; Wang, C.; Shao, B.; Wang, Z.; Xue, D.; Liu, Y.; Qi, K.; Yang, Y.; Niu, Y. *Anal. Chem.* **2017**, *89*, 12209−12216.
(26) Paterson, S.; de la Rica, R. *Analyst* **2015**, *140*, 3308−3317.
(27) Scognamiglio, V.; Arduini, F.; Palleschi, G.; Rea, G. *TrAC, Trends Anal. Chem.* **2014**, *62*, 1−10.

(28) Wu, M.; Lai, Q.; Ju, Q.; Li, L.; Yu, H. D.; Huang, W. *Biosens. Bioelectron.* **2018**, *102*, 256−266.
(29) Yan, X.; Li, H.; Su, X. *TrAC, Trends Anal. Chem.* **2018**, *103*, 1−20.
(30) Chen, G.; Zhu, J. Y.; Zhang, Z. L.; Zhang, W.; Ren, J. G.; Wu, M.; Hong, Z. Y.; Lv, C.; Pang, D. W.; Zhao, Y. F. *Angew. Chem., Int. Ed.* **2015**, *54*, 1036−1040.
(31) Guo, Y. M.; Zhang, L. F.; Zhang, S. S.; Yang, Y.; Chen, X. H.; Zhang, M. C. *Biosens. Bioelectron.* **2015**, *63*, 61−71.
(32) Nsibande, S. A.; Forbes, P. B. C. *Anal. Chim. Acta* **2016**, *945*, 9−22.
(33) Zhang, Z. P.; Zhou, H.; Mei, Q.; Wang, S.; Guan, G.; Liu, R.; Zhang, J.; Zhang, Z. *J. Am. Chem. Soc.* **2011**, *133*, 8424−8427.
(34) Kim, J. E.; Choi, J. H.; Colas, M.; Kim, D. H.; Lee, H. *Biosens. Bioelectron.* **2016**, *80*, 543−559.
(35) Kumar, A.; Kim, S.; Nam, J. M. *J. Am. Chem. Soc.* **2016**, *138*, 14509−14525.
(36) Zhao, X.; Xu, L.; Sun, M.; Ma, W.; Wu, X.; Kuang, H.; Wang, L.; Xu, C. *Small* **2016**, *12*, 4662−4668.
(37) Huang, X.; Song, J.; Yung, B. C.; Huang, X.; Xiong, Y.; Chen, X. *Chem. Soc. Rev.* **2018**, *47*, 2873−2920.
(38) Tang, J.; Xie, J.; Shao, N.; Yan, Y. *Electrophoresis* **2006**, *27*, 1303−1311.
(39) Deng, Y.; Cai, Y.; Sun, Z.; Liu, J.; Liu, C.; Wei, J.; Li, W.; Liu, C.; Wang, Y.; Zhao, D. *J. Am. Chem. Soc.* **2010**, *132*, 8466−8473.
(40) Vaisocherova-Lisalova, H.; Surman, F.; Víšová, I.; Vala, M.; Springer, T.; Ermini, M. L.; Šípová, H.; Šedivák, P.; Houska, M.; Riedel, T.; Pop-Georgievski, O.; Brynda, E.; Homola, J. *Anal. Chem.* **2016**, *88*, 10533−10539.
(41) Qu, Z.; Hu, F.; Chen, K.; Duan, Z.; Gu, H.; Xu, H. *J. Colloid Interface Sci.* **2013**, *398*, 82−87.
(42) Bastús, N. G.; Comenge, J.; Puntes, V. *Langmuir* **2011**, *27*, 11098−11105.
(43) Harimech, P. K.; Gerrard, S. R.; El-Sagheer, A. H.; Brown, T.; Kanaras, A. G. *J. Am. Chem. Soc.* **2015**, *137*, 9242−9245.
(44) Zhang, K.; Servos, M. R.; Liu, J. *J. Am. Chem. Soc.* **2012**, *134*, 7266−7269.
(45) Ma, X.; Tang, J.; Li, C.; Liu, Q.; Chen, J.; Li, H.; Guo, L.; Xie, J. *Anal. Bioanal. Chem.* **2014**, *406*, 5147−5155.
(46) Bhardwaj, N.; Bhardwaj, S.; Mehta, J.; Kim, K.; Deep, A. *Biosens. Bioelectron.* **2016**, *86*, 799−804.
(47) Hildebrandt, N.; Spillmann, C. M.; Algar, W. R.; Pons, T.; Stewart, M. H.; Oh, E.; Susumu, K.; Díaz, S. A.; Delehanty, J. B.; Medintz, I. L. *Chem. Rev.* **2017**, *117*, 536−711.